Shear testing of two aluminium alloys at different temperatures and strain rates

Author: Joacim Hagström

Report No.: [No] Swerea KIMAB Project No.: 523008 Date: 2008-01-24
Status: Open Member programme: 5

Modelling hot forming processes e.g. extrusion and hot rolling with high precision need reliable material property data. The experimental data need to come from tests at temperatures and strain rates close to the conditions that are to be modelled. It is also beneficial if the data are generated using the same material in the same condition and loaded in the same direction and mode as used in the processes that are to be modelled.

In this project all the criteria above were fulfilled for extrusion of two commercially important aluminium alloys, alloy AA6063 and AA6005A. The experimental set up was such that the material was tested in shear, which is the dominant deformation mode during extrusion. The strain rate was varied between 10^{-2}/s to $5x10^{+2}$/s and the temperature was varied from room temperature to 625°C.

Abstract

A new specimen geometry that makes it possible to make mechanical tests in shear at high strain rates and at high temperatures has recently been developed and evaluated at Swerea KIMAB [1].
In the present work the specimen geometry was changed to improve stability and thus reduce deformation of the specimen outside the shear zone. This report presents data from tests on two commercially important aluminium alloys, alloy AA6063 and AA6005A. Strain rate was varied between 10^{-2}/s and $5x10^{+2}$/s and the temperature was varied from room temperature to 625°C. The specimen geometry before and after mechanical testing was characterised using light optical microscopy. Microstructures were characterised using SEM and EBSD.
A comparison between shear testing and compression testing has been made which showed that the equivalent flow stresses became lower in shear than in compression with increasing strain. Some effect may be due to rotation of grains to softer texture components during shear deformation, and towards harder texture components during compression. It is important to restrict the measurements to deformations below the point where the geometry deviates from an ideal shear situation and develops cracks, even before the maximum force was reached. The point deviation from ideal shear deformation could be identified reasonably certainly in the elevated temperature tests. This new method offers some advantages for application to FEM modelling.

[Empty page]

Table of Contents

[Table of contens or emty page]

1. Introduction

Modelling hot forming processes such as extrusion and hot rolling with high precision need reliable material property data. The experimental data should ideally come from tests at temperatures and strain rates close to the conditions that are to be modelled. It is also beneficial if the data are generated using the same material in the same condition and loaded in the same direction and mode as used in the processes that are to be modelled.

In this project all the above criteria were fulfilled for extrusion of two commercially important aluminium alloys, alloy AA6063 and AA6005A. The experimental set-up was such that the material was tested in shear, which is the dominant deformation mode during extrusion. The strain rate was varied between 10^{-2}/s to $5x10^{+2}$/s and the temperature was varied from room temperature to 625°C.

A new specimen geometry that makes it possible to make mechanical tests in shear at high strain rates and at high temperatures has recently been developed and evaluated at Swerea KIMAB [1]. This specimen geometry was used to extract material property data for two aluminium alloys for modelling hot forming purposes. During the evaluation of these results it was found that the specimen deformed plastically also outside of the shear zone. It was possible to include this plastic deformation during analysis, but this was not the ideal solution. In the present work the specimen geometry was changed to improve stability and thus reduce the deformation of the specimen outside the shear zone.

2. Experimental setup

The material that was tested came from homogenized press bolts of alloys AA6063 and AA6005A. The materials chemistry and mechanical properties, as given from SAPA, are given in Table 1 and 2 below.

Table 1. Chemical contents and identification of the alloys.

Alloy designation	Sample designation	ST nummer	Charge	Si	Fe	Cu	Mn	Mg	Cr	Zn	Ti
AA6063	P07-0529	AK3081	070317-5A	0,43	0,20	0,007	0,048	0,45	<0.001	0,005	0,015
AA6005A	P07-0530	AK3082	703343	0,62	0,22	0,075	0,141	0,55	<0.001	0,003	0,016

Table 2. Mechanical properties, tensile testing.

Alloy designation	Sample designation	Rp0,2 (MPa)	Rm (MPa)	A (%)	n1
AA6063	P07-0529	77,3	172	22,9	0,258
AA6063	P07-0529	75,6	173	22,9	0,260
AA6005A	P07-0530	66,0	168	19,8	0,235
AA6005A	P07-0530	67,4	170	18,6	0,238

The yield strength was low for both materials, but not as low as the annealed temper given in handbooks [2,3,4]. The yield strength in the annealed temper is specified to 50 MPa and 55 MPa for these two alloys (AA6063 and AA6005A respectively). In the present case both alloys had higher strength values than given in handbooks, furthermore alloy AA6005A showed a lower yield strength (67 MPa) than the less alloyed AA6063 (76 MPa). The reason for this could be that a more complete precipitation of the solute elements had occurred in alloy AA6005A. The driving force for precipitation was larger

for the AA6005A alloy during heat treatment due to the higher alloying content, which gave more particles which, accordingly, resulted in smaller diffusion distances and therefore a more complete precipitation of the solute elements. The large particles give little strengthening and thus the more pure aluminium matrix gave the lower yield strength. The tensile strength was about equal for the two alloys (close to 170 MPa). The strength in the full hard condition (temper T6) for the alloys are (Yield Strength/Tensile Strength) 170/215 MPa and 240/270 MPa for AA6063 and AA6005A respectively [4]. The relatively low strength indicates that the ingots cooled down slowly from the homogenisation treatment which resulted in material with a matrix of (relatively) pure aluminium and large spheroidised particles.

SAPA Technology delivered 60 "raw" specimens, as solid cylinders of each alloy, 28 mm high with 80 mm in diameter. The specimens were machined so that the specimen height was parallel to the bolt press direction. The specimens' final geometry was machined in the KIMAB workshop.

Testing was performed using a hydraulic materials testing rig, specially designed for high speed testing. The maximum ram velocity was 1000 mm/s and with a special high speed PC card it was possible to log data with a frequency of 10^7 Hz.

2.1 Specimen geometry

The specimen design that was used in the preceding project [1] is presented in Figure 1. It was found that these specimens deformed plastically also outside of the shear zone which was undesired. The outer ring tilted somewhat and the height of both the outer ring and the inner cylinder decreased during testing. Simulations (using Q-form) reproduced these plastic deformations and predicted that the height of the inner cylinder (close to the gap) had decreased by 0.17 mm to 17.83 mm at the beginning of fracture. The outer ring had deformed so that the height was 23.93 mm close to the gap, i.e the height had decreased 0.07 mm. The gap decreased by 0.052 mm at the level of the inner cylinder top surface. Furthermore, the inner radius of the outer ring decreased by 0.067 mm. Actual measurements on deformed samples showed similar plastic deformations to the model predictions.

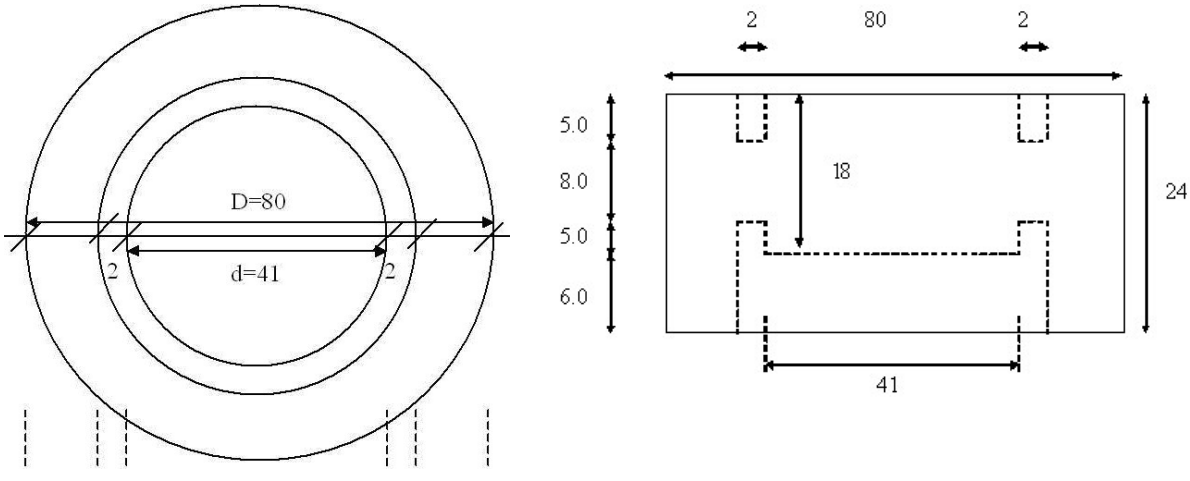

Figure 1. Specimen used in proceeding project [mm].

Several new geometries were simulated and a new geometry was then decided upon (Fig. 2). Three main rules were followed when the new geometry was chosen:

- The height up to the shear zone should be as small as possible, higher "legs" give more tilting tendency.
- The outer ring height above the shear zone should be higher, higher ring gives less tilting tendency.
- Larger ring wall thickness gives less tilting tendency.

Simulations of the new geometry showed that the unwanted plastic deformation outside the shear zone should be reduced considerably. The outer ring tilted somewhat and the height of both the outer ring and the inner cylinder decreased during testing. Simulations (Q-form) confirmed these plastic deformations and gave the results that, at the beginning of fracture, the gap decreases 0.005 mm at the level of the inner cylinder top surface. The inner radius of the outer ring decreases 0.018 mm and the height should be 23.98 mm close to the gap, i.e the height had decreased 0.018 mm.

Another factor for the development of the specimen geometry was temperature stability in the shear zone. The material between the tool and the shear zone acts as a buffer that decreases the temperature loss during testing, therefore the outer ring height was kept quite large. In Fig. 2 b) a schematic image of how the specimens were made from the extrusion billet is shown.

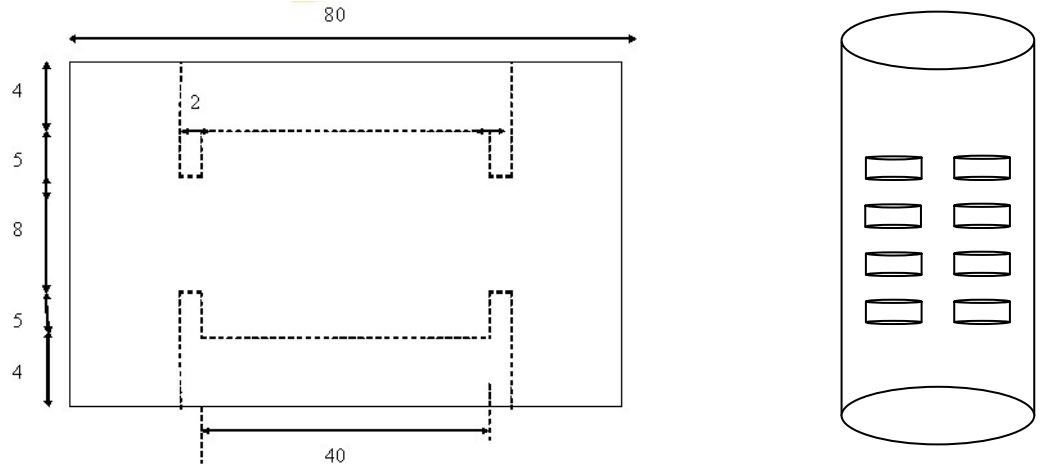

Figure 2. a) Specimen used in the present project [dimensions in mm].
b) Schematic image of how the specimens were made from the extrusion billet.

2.2 Testing philosophy

The principle of testing was that simple shear deformation is accomplished by pressing the inner cylinder downwards through the outer ring (see Figures 1 and 2). The testing was done with 6 different tool speeds at room temperature; 0.02 mm/s, 0.2 mm/s, 2 mm/s, 20 mm/s, 200 mm/s, and 1000 mm/s, giving shear strain rates of 0.01/s, 0.1/s, 1/s, 10/s, 100/s, 500/s. At high temperatures the testing was performed only at the four highest strain rates (1/s, 10/s, 100/s, 500/s).

Testing at high temperatures (450°C, 500°C, 550°C, 600°C, 625°C), was accomplished by first heating the specimens in an electrically heated muffle furnace. One specially made specimen with a hole drilled from the side and a thermo-couple attached in the hole was used as high performance thermometer. The furnace was loaded with 10 specimens from each alloy (two tests at each speed plus two extra as a precaution) and then heated to the testing temperature. When the temperature was stable at the desired testing temperature the specimens were retained for a further 1 hour. Then one specimen was removed from the furnace, quickly placed in the test rig and immediately tested using the chosen speed. Then this specimen was removed and the next specimen was tested, etc. All specimens for that actual temperature were tested in sequence; then the furnace was loaded with new specimens and the new temperature was selected. After each opening of the furnace the temperature dropped a few degrees, and the next specimen was not taken out until the correct testing temperature was re-established. The time between removing the specimen from the heating furnace until it was tested was always less than 5 seconds. The tools were not actively heated.

The specially made specimen with a thermo-couple attached in the drilled hole was used to measure the temperature drop profile when the specimens were removed from the furnace. The hole was drilled from the side of the specimen, direction towards the specimen centre to a depth of 19.5 mm and ended just in the wall where the shear zone is. The cooling rate in free air was logged manually and Table 3 shows how the temperature varied with time. During the first 10 seconds the temperature dropped about 7-10° (<1°/s), then the cooling rate decreased at longer times. A higher start temperature gave larger cooling rate in the beginning. Since the time that passed from the moment the specimen was removed from the heat until it was tested was less than 5 seconds, the temperature drop was less than 4° during the whole testing procedure.

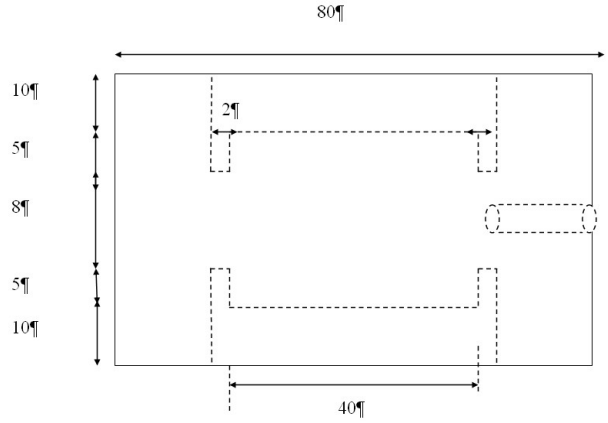

Figure 3. The special specimen used for temperature and cooling rate measurements in the present project. [dimensions in mm].

Table 2. Cooling rate in free air for the shear zone after removal from heating source

Start temp.	Time (s)	0	5	10	15	20	25	30	40	50	60
450 °C	Temp. (°C)	450	447	443	440	436	433	430	424	418	413
Start temp.	Time (s)	0	5	10	15	20	25	30	40	50	60
600 °C	Temp. (°C)	605	597	593	589	585	581	578	571	563	560

3. Results

3.1 Specimen geometry stability

Detailed measurements on the machined specimens before testing showed that the gap was wider at the entrance (2.3 mm) than at the bottom (2.1 mm), Figure 4 a, b). The depth of the gap was 5.05 mm.

Measurements on un-deformed specimens and specimens deformed at room temperature at all speeds show that the specimen geometry was very stable at room temperature. At high temperatures the specimens deformed more. The table below gives geometry changes during testing.

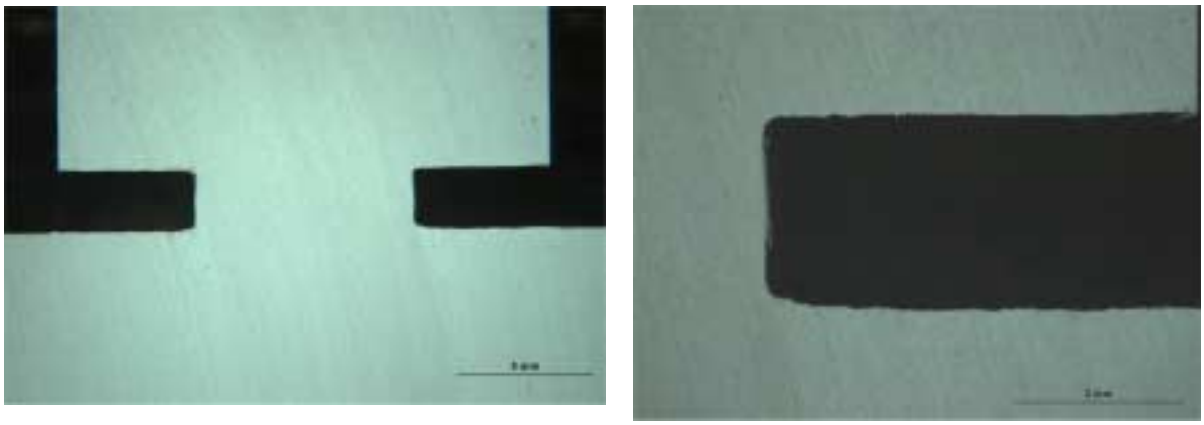

Figure 4 a, b. Machined specimen before testing. Specimen tilted 90° compared to Figure 2 in the images above, the test direction is thus horizontal.

Table 2. Geometry changes during testing

Test temp. (°C)	Strain rate (1/s)	detail	Position	Before test (mm)	After test (mm)	Difference (mm)
20	1	Outer radius	up	79,98	79,93	0,05
			down	79,98	80,00	-0,02
		Inner radius	up	44,38	44,34	0,04
			down	44,38	44,44	-0,06
	10	Outer radius	up	79,98	79,93	0,05
			down	79,98	80,00	-0,02
		Inner radius	up	44,38	44,34	0,04
			down	44,38	44,45	-0,07
	100	Outer radius	up	79,98	79,92	0,06
			down	79,98	80,00	-0,02
		Inner radius	up	44,38	44,31	0,07
			down	44,38	44,45	-0,07
500	1a	Outer radius	up	79,98	79,85	**0,13**
			down	79,98	80,24	**-0,26**
		Inner radius	up	44,38	44,23	**0,15**
			down	44,38	44,73	**-0,35**
	1b	Outer radius	up	79,98	79,85	**0,13**
			down	79,98	80,15	**-0,17**
		Inner radius	up	44,38	44,25	**0,13**
			down	44,38	44,68	**-0,30**

3.2 Shear test results

Specimens tested at room temperature and at elevated temperature are shown in Figs. 5 and 6 below. Examples of stress-strain curves are presented in Figs. 7 and 8. The stress and strain data from experiments were calculated from the load (kN) and position (mm) as measured from the MTS materials test rig. The built in load cell in the MTS rig is very accurate but was not constructed for high speed testing. Therefore a specially built load cell was used that was mounted directly on the upper tool, as described earlier. The displacement was measured by logging the test rig cylinder position. Small elastic deformations in the test rig, tool and specimen give rise to deviations from the actual deformation of the specimen.

To verify that the logged displacement accurately described the specimen deformation a comparison was made between plastic shear strain as measured on tested specimens and the logged data (force and displacement). Tested specimens were cut apart and polished and finally measured using light optical microscopy and relevant software. One problem was that the displacement (or shear strain) varied, depending whether the shear strain was measured on the upper or lower part of the shear zone. It was always the case that the strain measured on the upper part was smaller than the lower part, see Figures 5 and 6. For the specimens tested at room temperature the difference was small, and the specimens had totally collapsed so that complete fracture had occurred (Fig. 5). In the high temperature tests the specimens had not fractured completely and it was possible to analyse the plastic strain from LOM images. The difference in measured (apparent) strain was quite substantial as can be seen in Fig. 6 a). In Figs. 6 b) and 6 d) it is clearly seen that, at the upper part, the material from the shear zone has merged to the inner cylinder and a crack has developed. This phenomenon was not seen in the lower part of the shear zone.

The curved surfaces are partly related to the variation in cross-section from inside to outside of the sheared ring. The cross-sectional area is smaller at the inside, which results in larger stresses and initiation of deformation therefore start at the inside of the sheared ring. When the work hardening rate is low at high strains a small difference in stress could give a large difference in strain.

To further investigate the fracture mechanisms and to try to understand at which point in the stress-strain curve fracture occurred new experiments were performed. Two new tests were done at room temperature, one with less strain (1.6 mm displacement) and one with slightly larger strain (1.9 mm displacement). Both tests were interrupted before the expected maximum load and subsequent plastic flow and fracture. No data was logged during these tests, and analysis was therefore only possible by studying cross-sections and by measuring the plastic deformation on the samples.

The specimens were then cut in pieces and the cross-sections were prepared for LOM imaging by polishing. To reveal the small cracks that can be seen in Figs. 7 a) – f) the cross-sections were electro-polished for 45 – 60 s in 10% solution of perchloric acid in methanol (20°C, 30 V). It is evident from the LOM images in Figs. 7 a) – f) that cracks and faults appeared before maximum loading in the shear tests. It was therefore vital for the test method to find out how to define where and when cracking had started. By studying the stress-strain curves for the warm tests it was possible to define a point where the stress increase started to decrease, see examples for both alloys in Figs. 8 and 9. This deflection point could be defined for the warm tests with good agreement to the measured strains

from LOM images on polished cross-sections. It was however more difficult to get reliable values for the room temperature tests since these tests did not show the same profile with a steady stress increase followed by a subsiding stress increase, Figs. 8 a) and 9 a).

For the room temperature tests cracks and voids occurred relatively early both at the lower and upper part of the shear zone which surely affected the flow stress, and the flow stress results can therefore probably not be trusted above a shear strain of 0.5. A factor of 0.7 could be calculated for the relation between the strain determined from the peak load in MTS rig and the strain measured from LOM images. This factor was used to evaluate the "strain at start of failure" by simply multiplying the strain at peak load with 0.7 (values presented in Tables 3 a) and 4 a)).

Table 3 and 4 a) – d) present mechanical properties in terms of shear stress and shear strains and Table 5 a) and b) gives parameters for an equation describing the flow stress in the form;

$$\tau_{pl} = \tau_0 + k\gamma_{pl}^n \qquad \text{Eq. 1}$$

Eq. 1 is valid up to the values given in tables 3 a) and 4 a) "strain at beginning of fracture", above this value fracture could have started by crack propagation. Eq. 1 was rewritten from the famous equation by Ludwig [5], given in Eq. 2. "n" was given the value 1 in this case. From this equation it is possible to calculate the flow stress at any plastic strain. In Table 6 parameters for von Mises normal stresses (σ) and strains (ε) are given calculated from Eq. 2.

$$\sigma_{pl} = \sigma_0 + k\varepsilon_{pl}^n \qquad \text{Eq. 2}$$

The strain rate behaviour of FCC metals can be described by Eq. 3 [5].

$$\sigma_2 = \sigma_1 + k\log\left(\dot{\varepsilon}_2 / \dot{\varepsilon}_1\right) \qquad \text{Eq. 3}$$

From the data in the present series of shear tests the constant in Eq. 3 was found to be equal to 5 for both alloys.

Furthermore, the temperature dependence of σ can be described with the help of the homologue temperature, Eq. 4.

$$T^* = \frac{T - T_{ref}}{T_{melt} - T_{ref}} \qquad \text{Eq. 4}$$

$$\sigma = \sigma_{ref}\left(1 - \left(\frac{T - T_{ref}}{T_{melt} - T_{ref}}\right)^m\right) \qquad \text{Eq. 5}$$

The flow stresses as derived from experiments are compared calculated data using Eqs. 3 and 5 in Fig. 12 and 13.

It can be noted that the present test method appears to give reliable results that are not affected by crack formation up to shear strains in excess of 0.7 for the temperatures that are relevant to hot extrusion. The values of strain at failure suggest that the hot workability improves somewhat with increasing temperature in the range from 450 to 600°C (for alloy AA6063 also 625°C) and is rather insensitive to strain rate. At the highest temperature of 625°C the AA6063 continued to behave normally although the flow stresses became very small. However, no real values of flow stress applied for the AA6005A alloy, apparently due to the formation of liquid zones inside the material. This temperature had evidently exceeded the limit of hot workability for this alloy composition and microstructural state.

With additional tests at more closely spaced temperatures it should be possible to use this method to define the limit of hot workability as a function of temperature, strain and strain rate. It would be interesting to see whether the on-set of failure due to incipient melting and severe loss of hot workability could be detected in such tests at somewhat higher temperatures also for alloy AA6063.

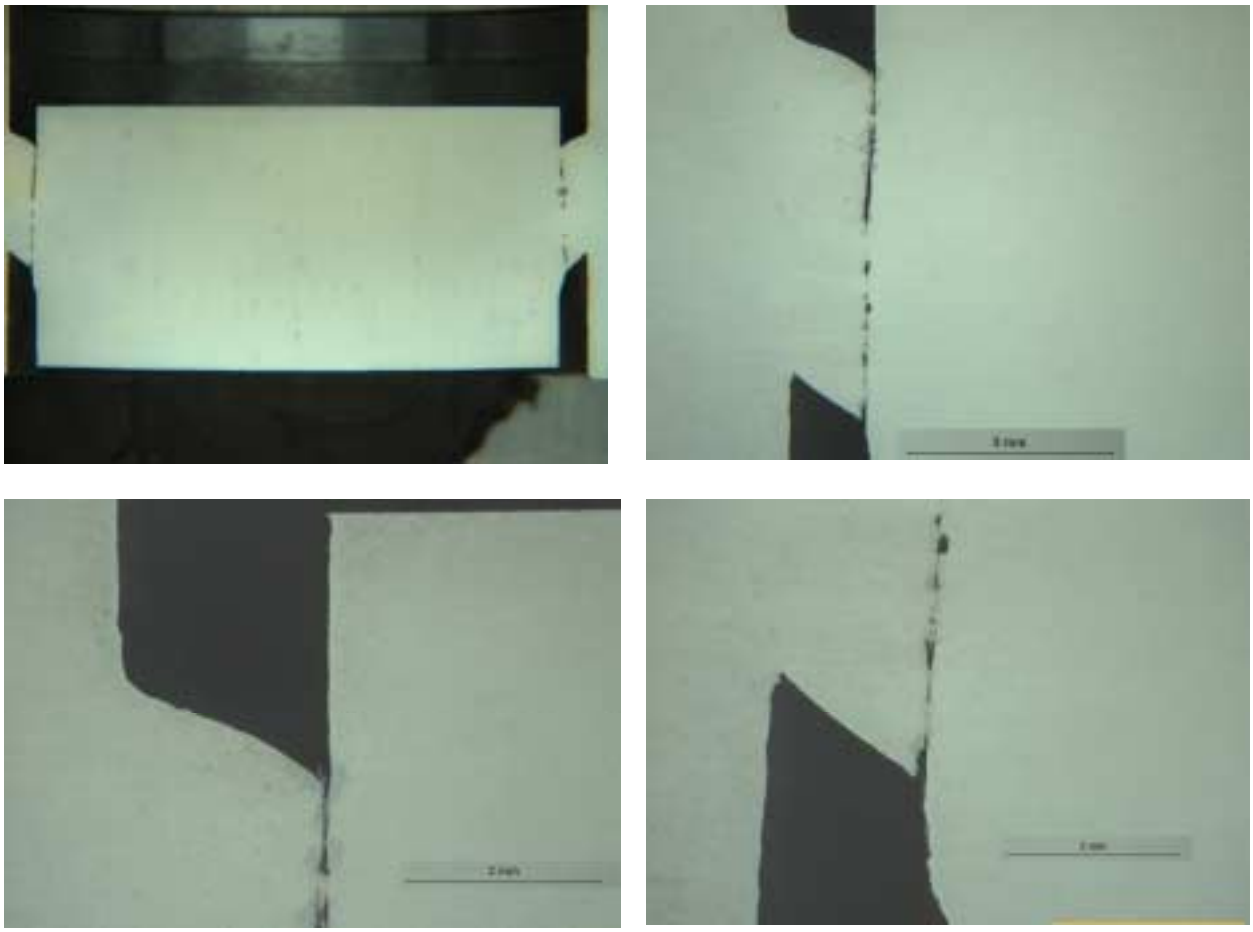

Figure 5 a-d. Cross section of a specimen after testing in room temperature with 1/s strain rate in different levels of detail. In a) both shear zones are visible and the inner cylinder as well. in b) the shear zone to the left is seen and in c) and d) the upper and lower parts of the shear zone are shown in more detail.

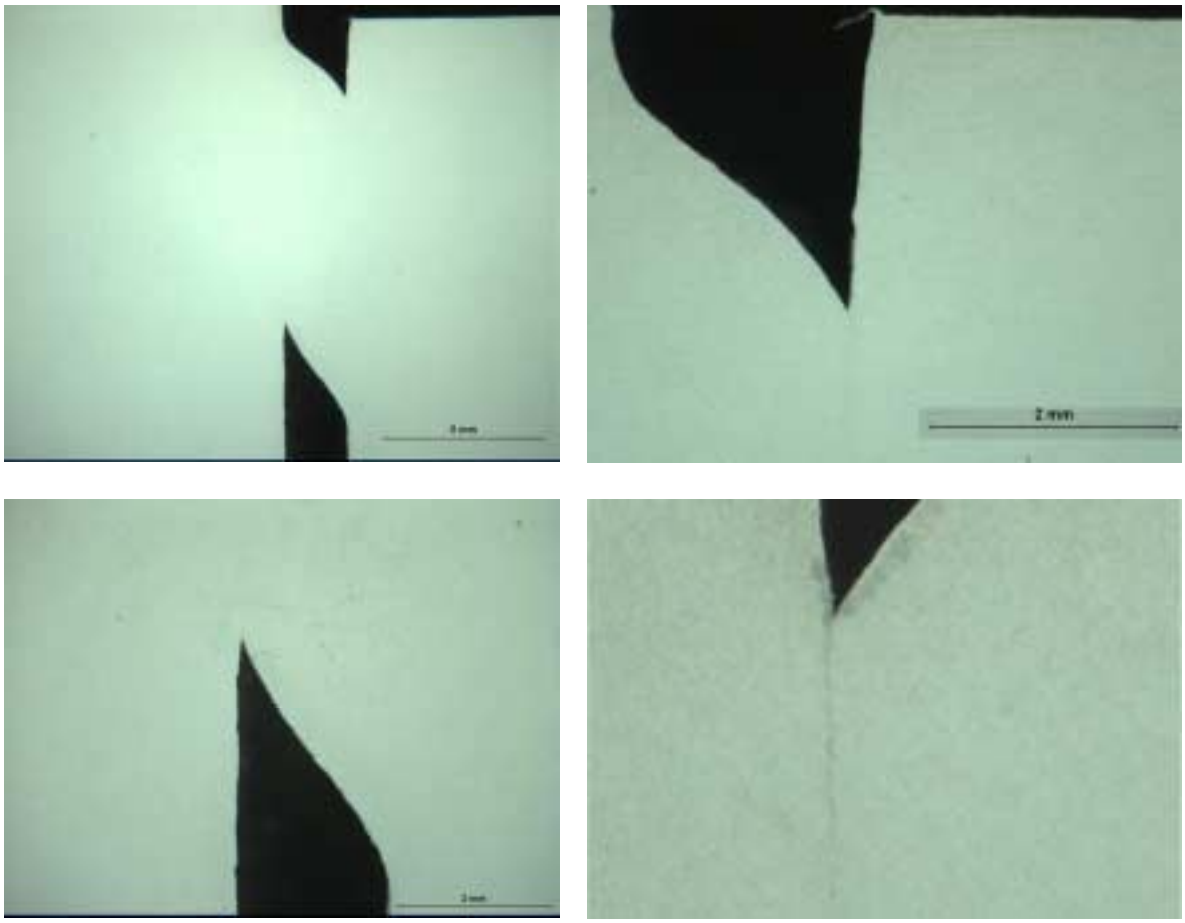

Figure 6 a-d. Cross section of a specimen (AA6063) after testing in high temperature (500°C) with 1/s strain rate in different levels of detail. In a) the whole shear zone is visible. In b) and c) the upper and lower parts of the shear zone are shown in more detail. In d) a crack is visible in a deformed AA6005A specimen (500°C, 1/s).

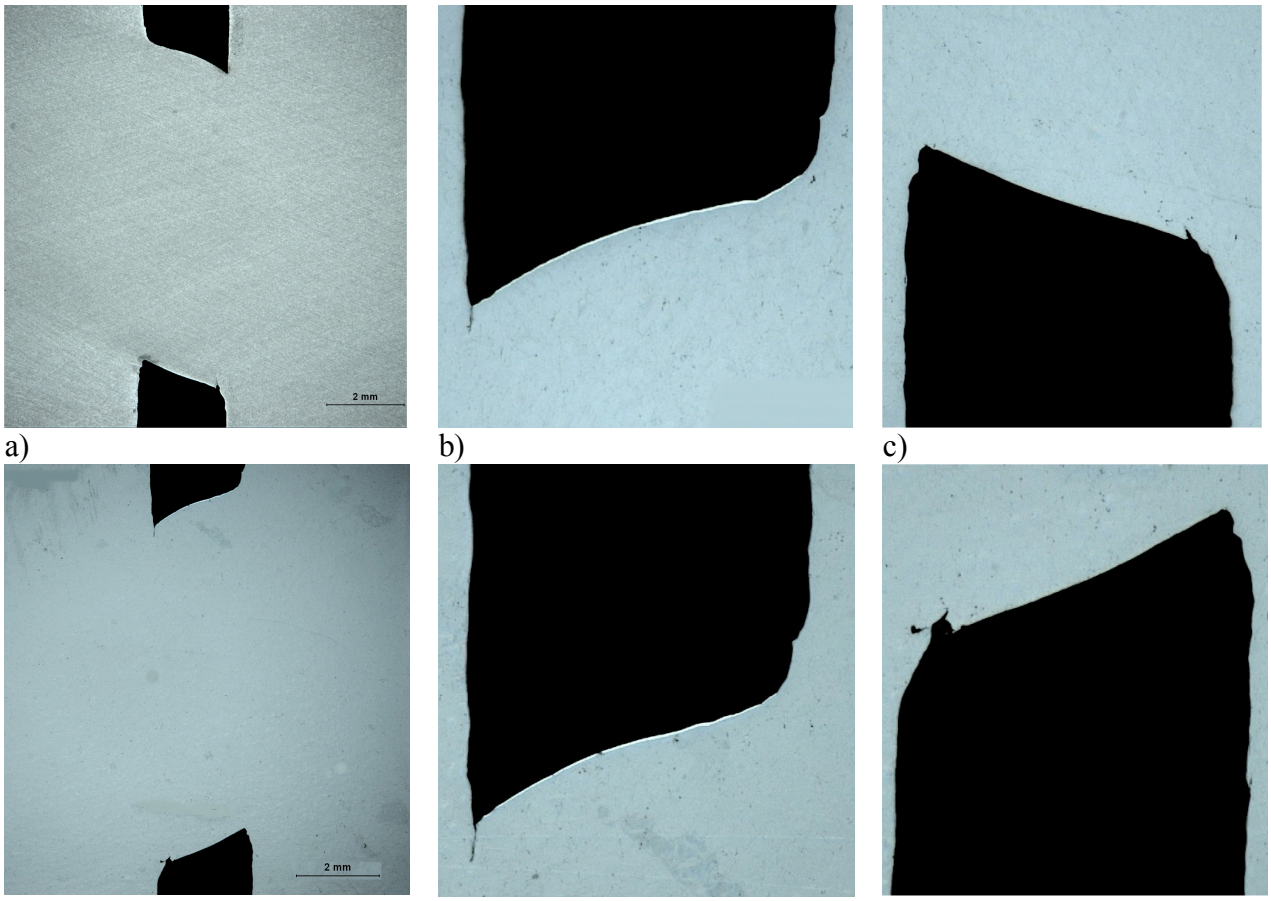

a) b) c)

d) e) f)

Figure 7 a) – f). Cross sections of specimens after testing in room temperature and interrupted before fully loaded.

a) Specimen with little strain, the whole shear zone is visible. Only mechanically polished and no crack is visible in the upper part. Failure in the lower part is visible though.

b) Upper part of the shear zone is shown in more detail. Cross-section electro-polished to reveal cracks.

c) Lower part of the shear zone is shown in more detail. Cross-section electro-polished to reveal cracks.

d) Specimen with more strain, the whole shear zone is visible. Cross-section electro-polished to reveal cracks.

e) Upper part of the shear zone is shown in more detail. Cross-section electro-polished to reveal cracks.

f) Lower part of the shear zone is shown in more detail. Cross-section electro-polished to reveal cracks.

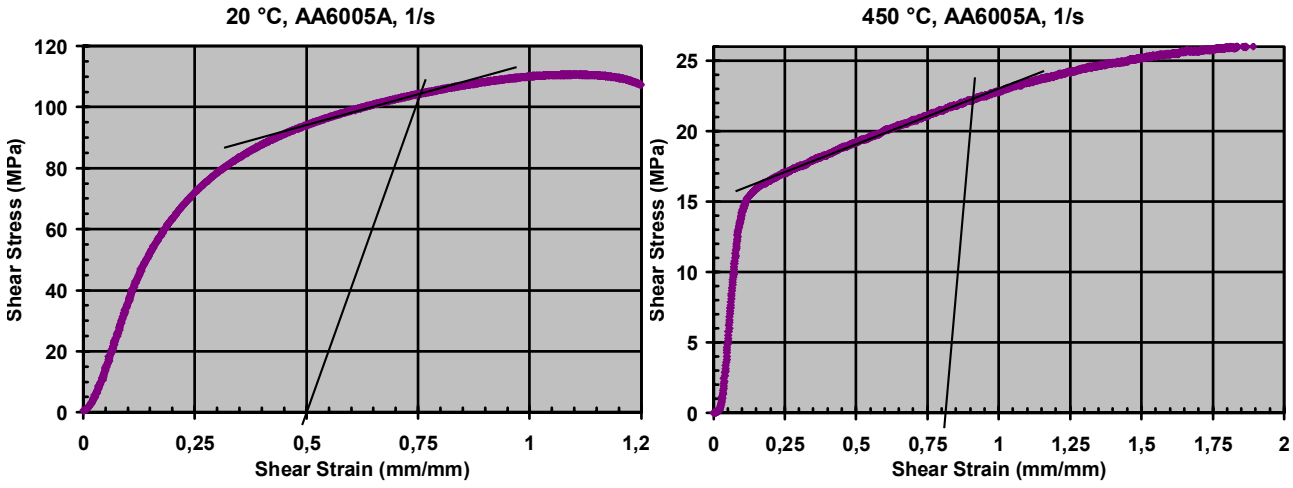

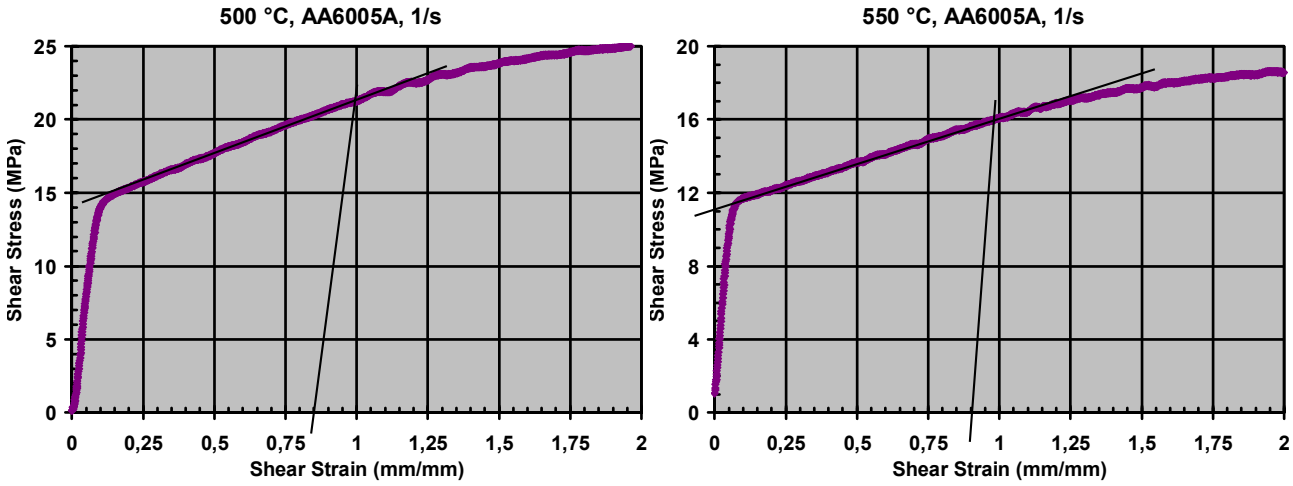

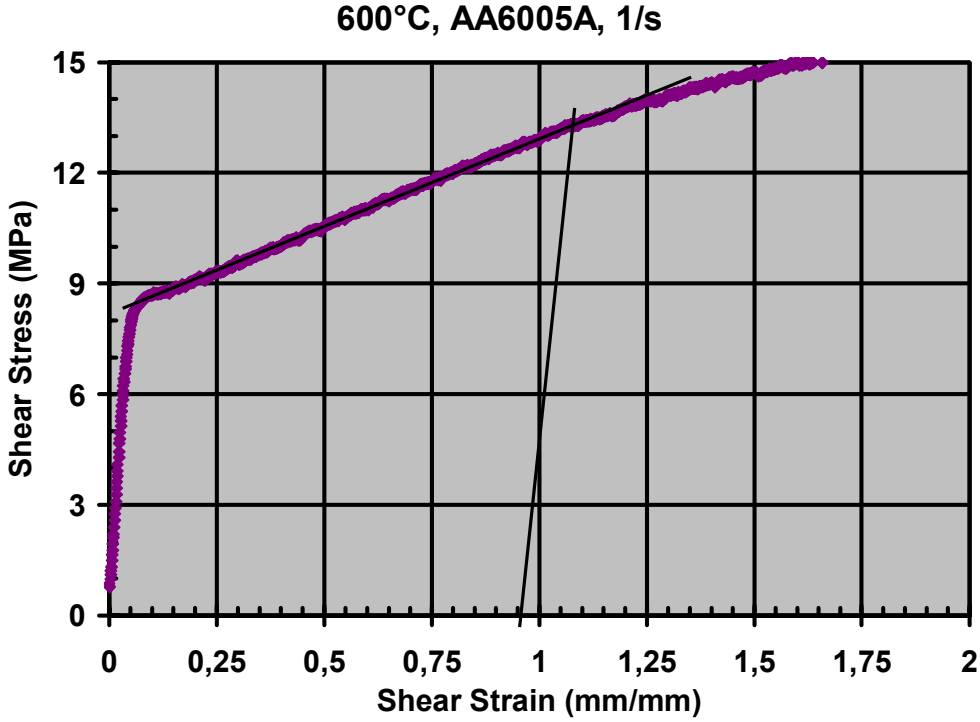

Figure 8 a) – e). Stress strain curves for alloy AA6005A at 1/s strain rate and different temperatures. Note that the scale is very different for the stress in the four figures.

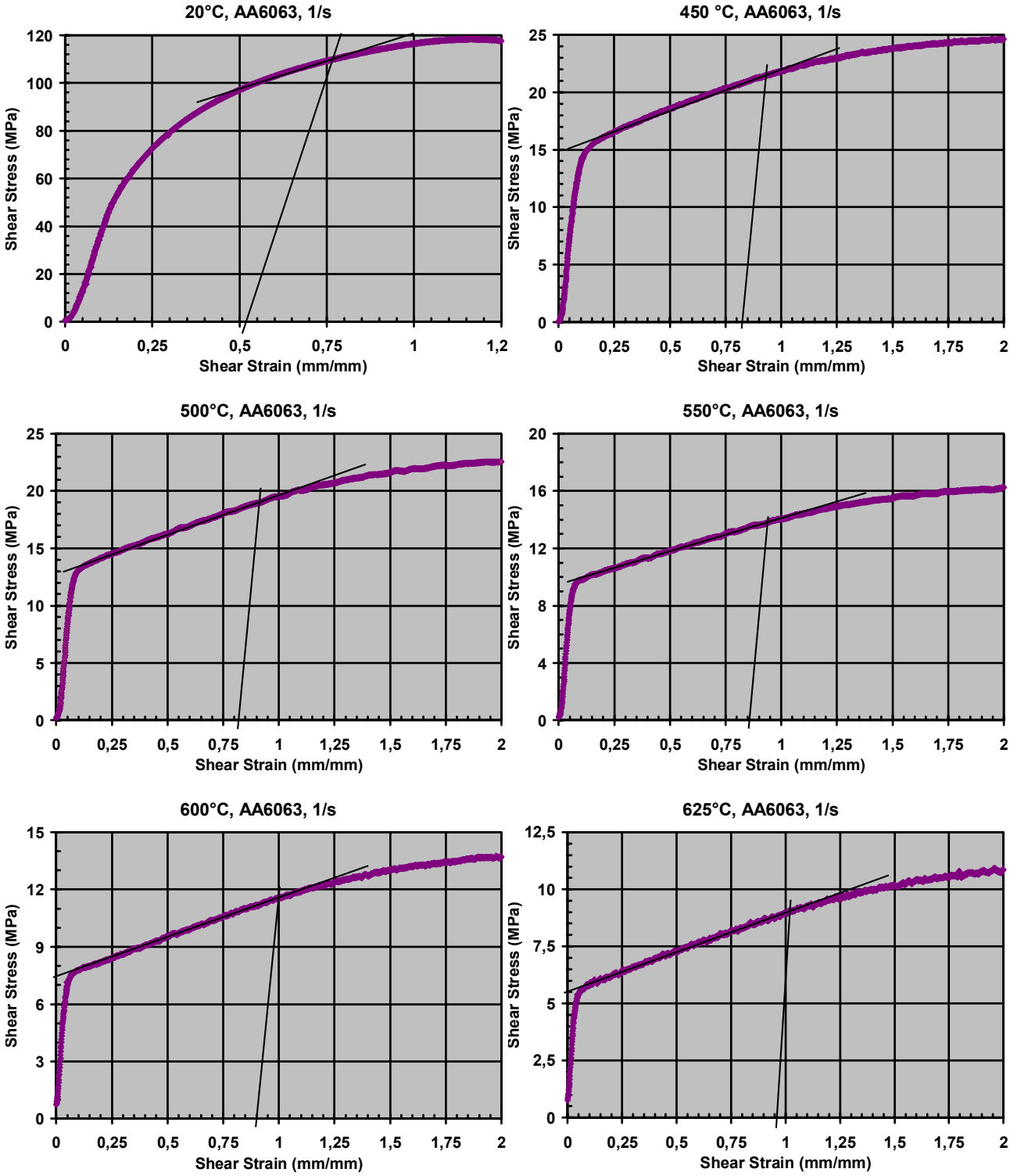

Figure 9 a) - f). Stress strain curves for alloy AA6063 at 1/s strain rate and different temperatures. Note that the scale is very different for the stress in the four figures.

Table 3a. Mechanical properties from shear tests. Alloy AA6005A,
Shear Strain at start of failure (mm/mm).

	Shear Strain Rate					
Temp. (°C)	0,01	0,1	1	10	100	500
25	0,50	0,50	0,50	0,55	0,55	0,55
450			0,80	0,75	0,75	0,75
500			0,85	0,80	0,80	0,80
550			0,90	0,85	0,85	0,85
600			0,95	0,90	0,85	0,85
625			-	-	-	-

Table 3b. Mechanical properties from shear tests. Alloy AA6005A,
Shear Flow Stress, 1 % plastic deformation (MPa).

	Shear Strain Rate (mm/mm/s).					
Temp. (°C)	0,01	0,1	1	10	100	500
25	48	49	49	50	50	50
450			14,5	17	19	-
500			13,5	17	18,5	-
550			11	15	-	-
600			8,25	11,5	15,5	19
625			-	-	-	-

Table 3c. Mechanical properties from shear tests. Alloy AA6005A,
Shear Flow Stress, 5 % plastic deformation (MPa).

	Shear Strain Rate (mm/mm/s).					
Temp. (°C)	0,01	0,1	1	10	100	500
25	65	66	67	67	67	67
450			16	21	23	25
500			14,75	20	22,5	24
550			11,5	16,5	22	22,5
600			8,75	12,5	18	21
625			-	-	-	-

Table 3d. Mechanical properties from shear tests. Alloy AA6005A,
Maximum Shear Stress in test (MPa).

	Shear Strain Rate (mm/mm/s).					
Temp. (°C)	0,01	0,1	1	10	100	500
25	109	110	111	112	112	115
450			26	26,25	33,5	38
500			24,5	23	30,5	36
550			18,5	18,5	25,5	31,5
600			15,75	14	22	27,5
625			-	-	-	-

Table 4a. Mechanical properties from shear tests. Alloy AA6063,
Shear Strain at break (mm/mm).

	Shear Strain Rate (mm/mm/s)					
Temp. (°C)	0,01	0,1	1	10	100	500
25	0,50	0,50	0,50	0,50	0,50	0,50
450			0,75	0,75	0,75	0,80
500			0,80	0,80	0,80	0,75
550			0,85	0,80	0,80	0,75
600			0,90	0,80	0,80	0,80
625			0,95	0,85	0,75	0,75

Table 4b. Mechanical properties from shear tests. Alloy AA6063,
Shear Flow Stress, 1 % plastic deformation (MPa).

	Shear Strain Rate (mm/mm/s)					
Temp. (°C)	0,01	0,1	1	10	100	500
25	49	50	53	53	-	-
450			11,5	16,5	17,5	-
500			12	15	16,5	-
550			9	12,5	-	-
600			7	10,5	12,5	14
625			5,25	9	12,5	12,5

Table 4c. Mechanical properties from shear tests. Alloy AA6063,
Shear Flow Stress, 5 % plastic deformation (MPa).

	Shear Strain Rate (mm/mm/s)					
Temp. (°C)	0,01	0,1	1	10	100	500
25	64	64	68	69	-	-
450			14,5	19,5	22	23
500			13,5	17,5	20	21
550			9,75	14	19	19
600			7,75	11,25	14,5	17
625			5,75	9,5	14	14,5

Table 4d. Mechanical properties from shear tests. Alloy AA6063,
Maximum Shear Stress in test (MPa).

	Shear Strain Rate (mm/mm/s)					
Temp. (°C)	0,01	0,1	1	10	100	500
25	117	118	119	120	120	122
450			24,25	25	32	36
500			22	21	27,5	32,5
550			16	16,5	23,5	27
600			13,5	13,5	18,75	24,5
625			11	11	16,25	19,5

Table 5 a. Alloy AA6005A, parameters for an equation describing the flow stress in the form; $\tau_{pl} = \tau_0 + k\gamma_{pl}$. T=temperature (°C), S R = Strain Rate (s^{-1}).

Tau - zero					k1				
T / S R	1	10	100	500	T / S R	1	10	100	500
450	16	22,25	28,5	30	450	8	4	4,8	8
500	14,5	20,5	27	27,5	500	7,3	2,8	4,6	8
550	11,5	16,5	23,5	25	550	5	1,8	2,8	7,5
600	8,5	12,5	20	22	600	4,7	1,2	2	6,5
625	-	-	-	-	625	-	-	-	-

Table 5 b. Alloy AA6063, parameters for an equation describing the flow stress in the form; $\tau_{pl} = \tau_0 + k\gamma_{pl}$. T=temperature (°C), S R = Strain Rate (s^{-1}).

Tau - zero					k				
T / S R	1	10	100	500	T / S R	1	10	100	500
450	15,5	21	27	27	450	7,3	4	6	9,3
500	13	18	23	23	500	6,6	2,9	5,6	9
550	9,75	14,25	21	21	550	5,1	2	4	7,3
600	7,75	12	17	18	600	4	1,3	2,3	6,4
625	5,75	9,5	15,5	16	625	3,5	1,25	1,6	5

Table 6 a. Alloy AA6005A, parameters for an equation describing the flow stress (normal stresses and strains) in the form; $\sigma_{pl} = \sigma_0 + k\varepsilon_{pl}^n$. T (°C), SR=Strain Rate (s^{-1}).

Sigma - zero					k1				
T / S R	1	10	100	500	T / S R	1	10	100	500
450	27,5	38	50	52	450	8	4	4,8	8
500	25,5	35	47	47	500	7,3	2,8	4,6	8
550	20	28,5	41	43,5	550	5	1,8	2,8	7,5
600	14,5	22	35	38,5	600	4,7	1,2	2	6,5
625	-	-	-	-	625	-	-	-	-

Table 6 b. Alloy AA6063, parameters for an equation describing the flow stress (normal stresses and strains) in the form; $\sigma_{pl} = \sigma_0 + k\varepsilon_{pl}^n$. T (°C), SR=Strain Rate (s^{-1}).

Sigma - zero					k				
T / S R	1	10	100	500	T / S R	1	10	100	500
450	27	36	46,5	47,5	450	21,4	12,9	18,7	25,4
500	23	31	40	40	500	21,25	10	15,8	17,1
550	17	25	36,5	36,5	550	15,8	6,4	14,2	21,4
600	12,75	20,75	29	32	600	13,3	5	8,6	17,5
625	9,5	17,5	26,75	27,5	625	10,5	5,3	7	16,8

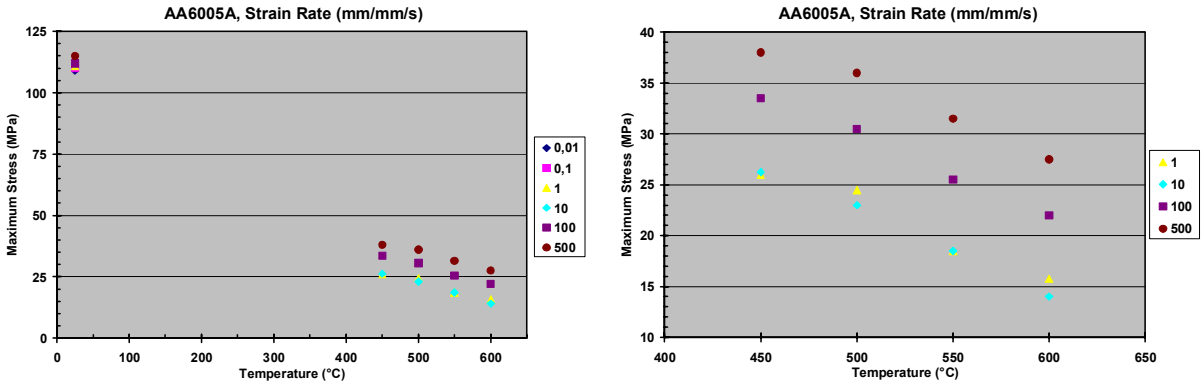

Figure 10 a, b. Largest measured shear stress (MPa) plotted vs. temperature (°C) at different strain rates (mm/mm/s). Figure b) shows the right corner of a) in more detail.

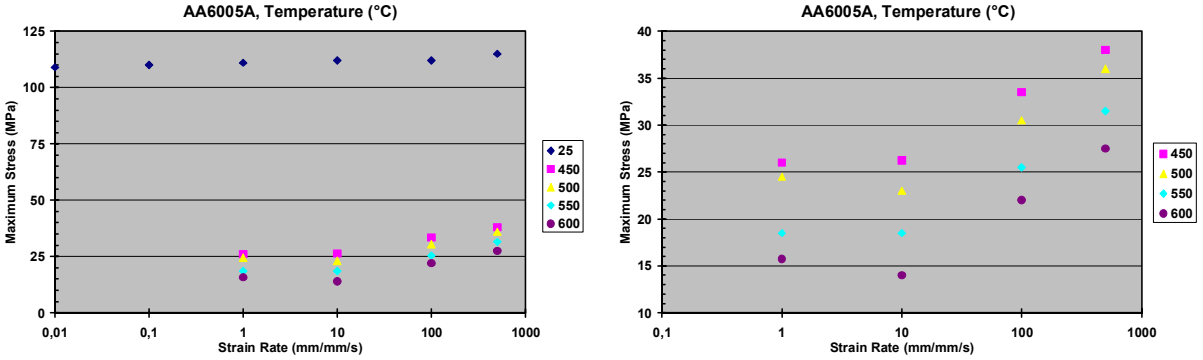

Figure 10 c, d. Largest measured shear stress (MPa) plotted vs. strain rate (mm/mm/s) at different temperatures (°C). Figure b) shows the right corner of a) in more detail.

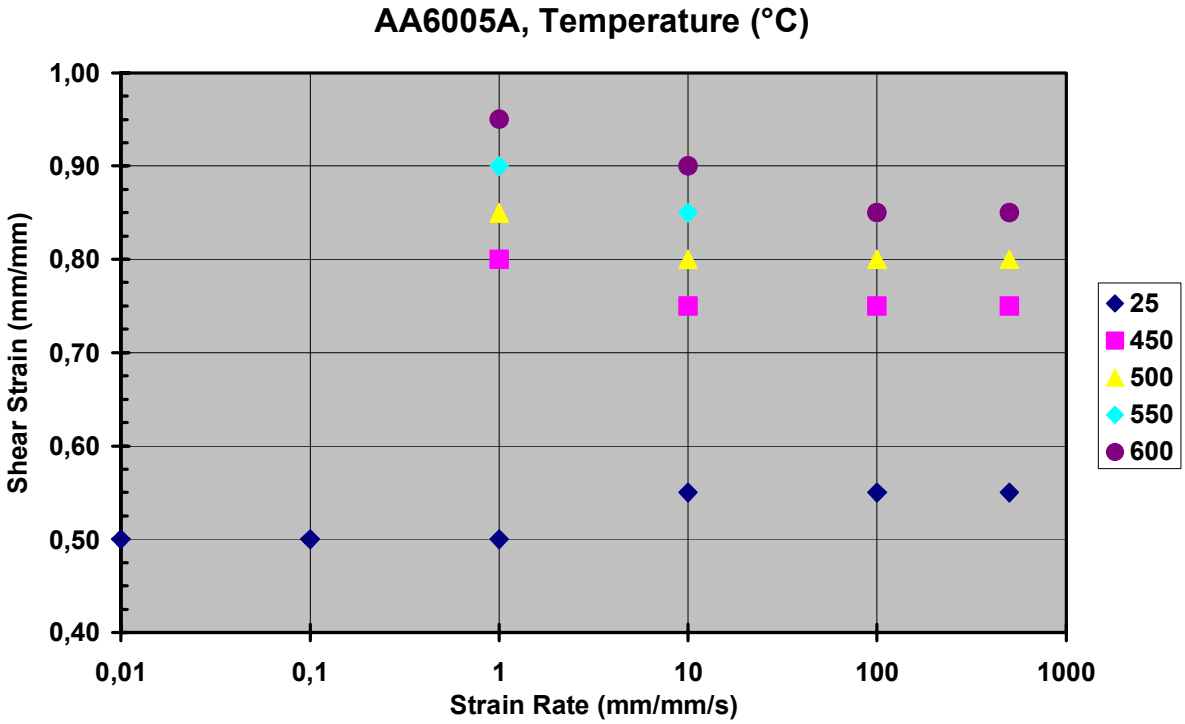

Figure 10 e. Shear strain (mm/mm) at crack initiation point plotted vs. strain rate (mm/mm/s) at different temperatures (°C).

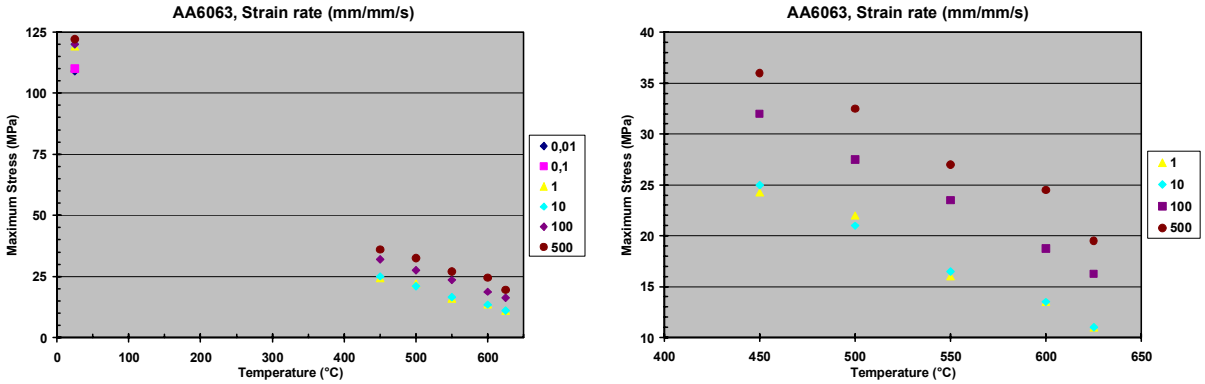

Figure 11 a, b. Largest measured shear stress (MPa) plotted vs. temperature (°C) at different strain rates (mm/mm/s). Figure b) shows the right corner of a) in more detail.

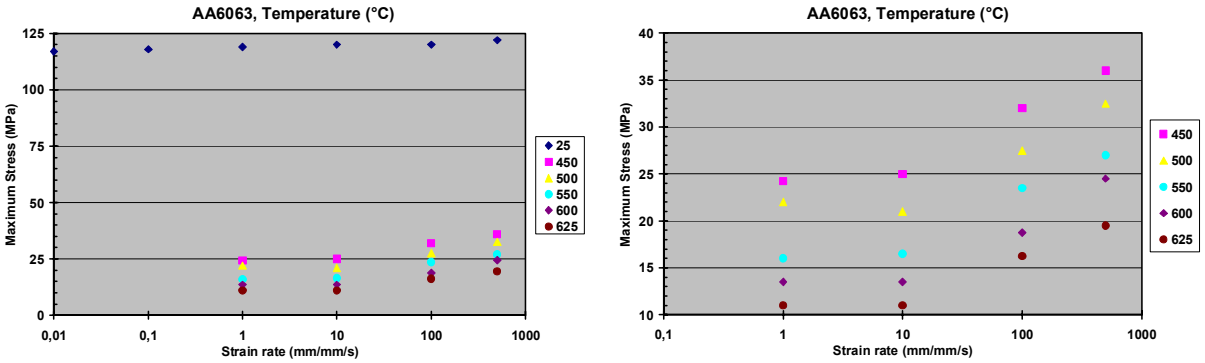

Figure 11 c, d. Largest measured shear stress (MPa) plotted vs. strain rate (mm/mm/s) at different temperatures (°C). Figure b) shows the right corner of a) in more detail.

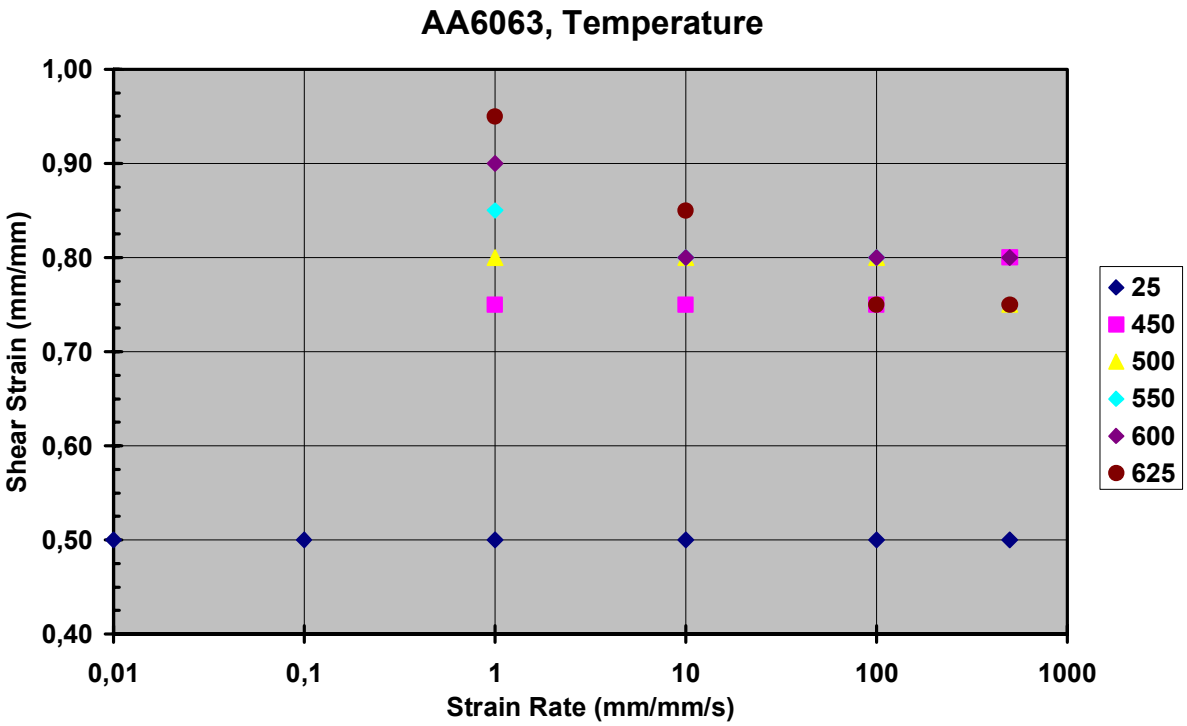

Figure 11 e. Shear strain (mm/mm) at crack initiation point plotted vs. strain rate (mm/mm/s) at different temperatures (°C).

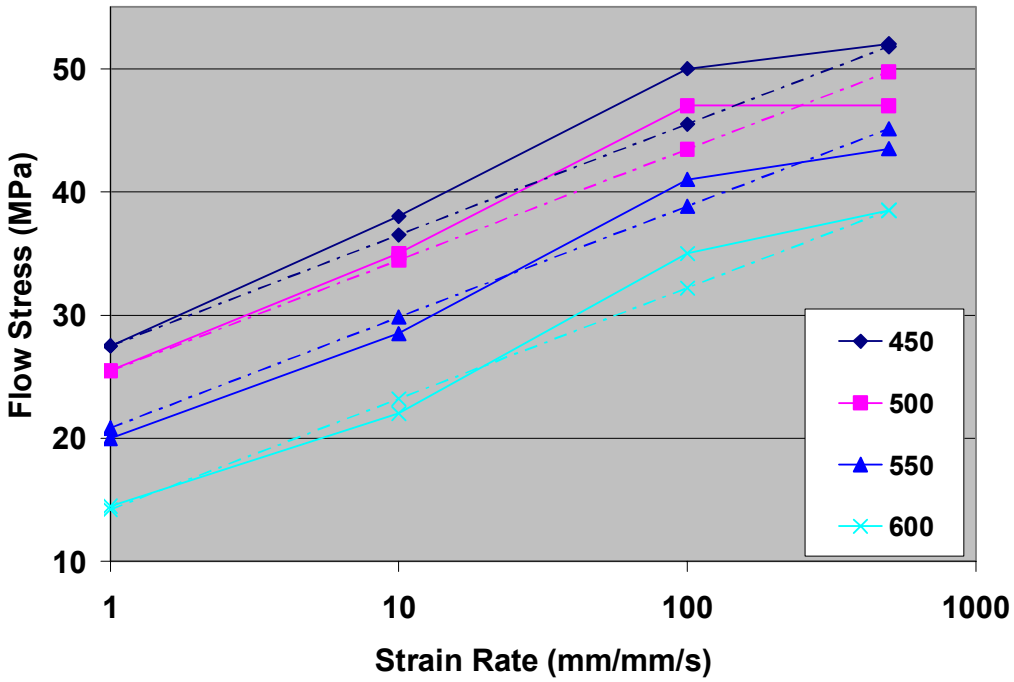

Figure 12. Alloy AA6005A, flow stress as derived from experiments are compared to calculated data using Eqs. 3 and 5.

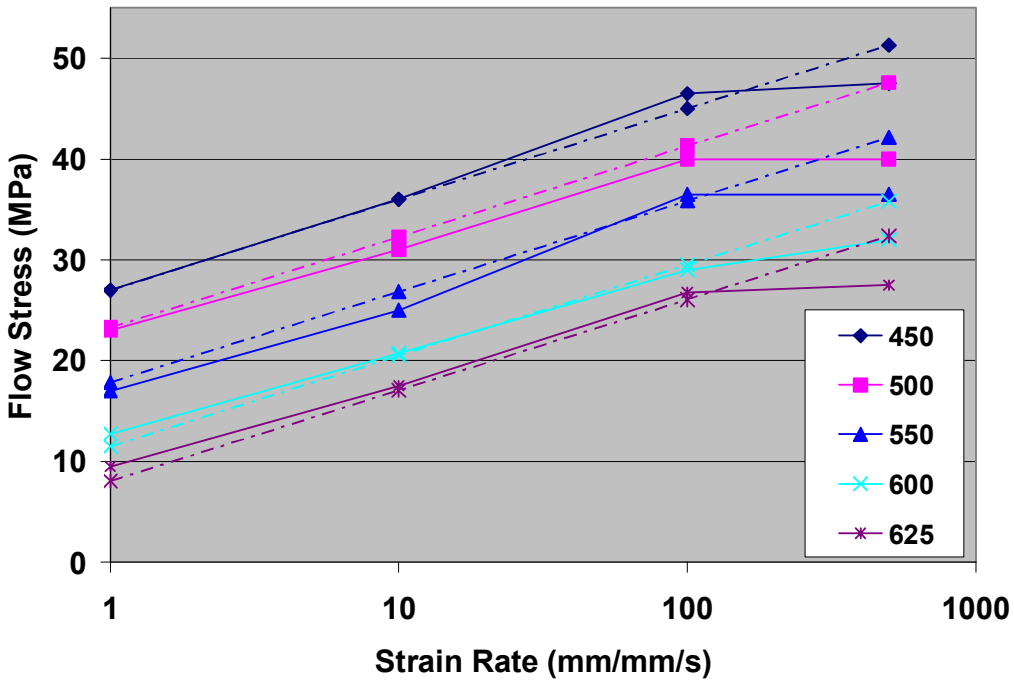

Figure 13. Alloy AA6063, flow stress as derived from experiments are compared to calculated data using Eqs. 3 and 5.

3.3 Compression test results and comparison with shear test results

Compression tests were made for comparison with the shear tests. Tests were done at room temperature, on both materials and in different directions, parallel to the billet length (index "S") and at right angles to the billet length (index "L"). Figures 12 a) and b) show the results of the compression testing and Figure 13 shows both the compression tests and shear tests in the same figure. The difference in flow stress between the two test directions indicates that the cast ingots contained some source of anisotropy. This is very surprising as the cast billets are generally assumed to have equi-axed structures that are completely random in crystallographic texture. Especially alloy AA6063 show a significant difference, 10 MPa which is about 4 %. This question deserves further study.

At the beginning of deformation, there is excellent agreement between the curves for the two test methods. However, they then diverge and the difference between compression testing and shear testing is 40 MPa at a true "effective" strain of 0.3, which correspond to about 20 % increase in strength when tested in compression compared to shear. Shear strain was recalculated to effective strain by dividing by the square root of 3 and shear stress was converted to effective stress by multiplication with the square root of 3, according to von Mises' theory of plastic flow. Part of the difference may be due to friction at the ends of the compression specimens which is not adequately compensated. Another part of the difference can be explained by the rotation of grains and sub grains during deformation. During compression rotation of crystallographic directions give rise to a <110> fibre texture that increases flow stress, but in the case of shear deformation the texture becomes a mixture of {111}<uvw> and {100}<011>, for which a softening is expected. Texture strengthening in common engineering materials can be described by the variation of the Taylor factor (M) with orientation. The M values are proportional to the yield stress of textured polycrystalline aggregates which have various <hkl> fibre axes along the tension or compression axes. In Ref [[6]] the M factors were calculated for cubic metals and plotted in a crystallographic unit triangle. The extremes are represented by <100> and <111> fibre textures and the latter is 50 % stronger than the former. Compared to a random distribution an introduction of a strong <111> or <110> texture would give a strengthening of about 20%. In practice, the degree of strengthening is considerably diluted by the spread of orientations that is present in the material and the total anisotropy of yield stress seldom exceeds 10 to 15 % [6]. Nevertheless, the development of deformation textures is probably a significant contribution to the difference in flow stress levels and it is worth recalling that much of the flow in extrusion is dominated by shearing. For this reason it may be expected that the present shear testing should give more relevant data than compression when applied to FEM modelling of the industrial process.

For room temperature deformation it was stated above that the shear strain, at which fracture in the form of crack initiation started, was 0.5. The normal strain was thus $0.5/\sqrt{3} = 0.29$. It is difficult to say to which point the results can be trusted in this case, but for effective strains above 0.3 it cannot be recommended to use the shear test result at room temperature. For the tests at elevated temperatures the shear strain, at which fracture in the form of crack initiation started, was larger than 0.5. The strains evaluated from LOM images indicates that fracture initiated at a shear strain of about 0.75 at 450°C and 0.9 at 600°C which correspond to von Mises effective strains of 0.43 and 0.52.

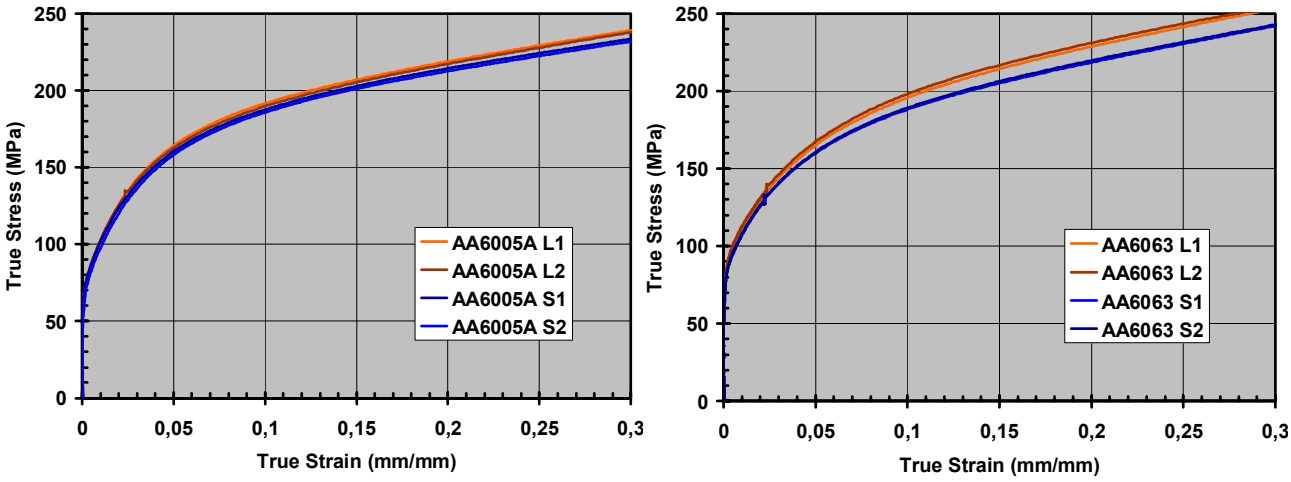

Figure 12 a, b. True stress – strain curves from compression tests for alloy AA6005A (a) and AA6063 (b). Specimens with index "S" were tested with the deformation direction parallel to the billet length and specimens with index "L" at right angels to the billet length.

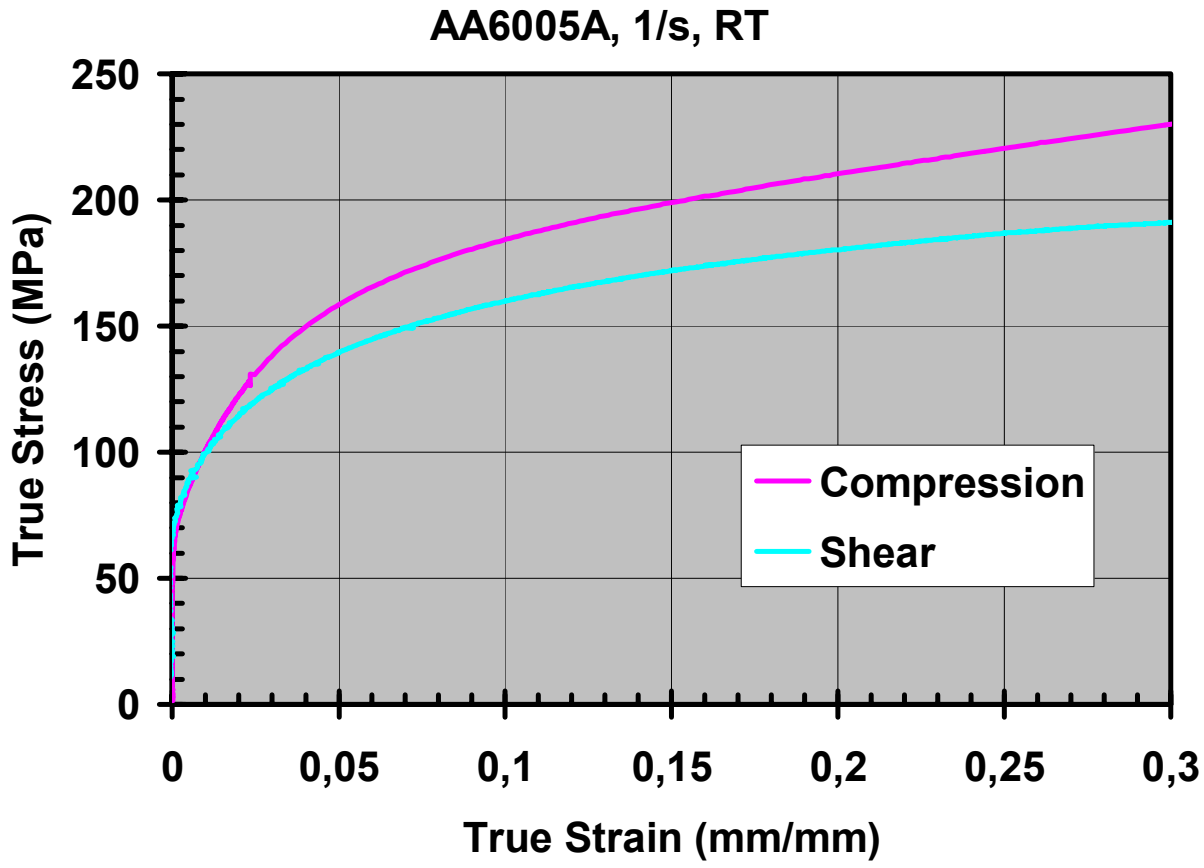

Figure 13. True stress – strain curves from shear and compression tests for alloy AA6005A. Shear strain and shear stress recalculated to "normal" strain and "normal" stress (V. Mises).

4. Microstructure

Microstructures in not-deformed material and in sheared regions have been characterised using electron back-scattering diffraction (EBSD) in the scanning electron microscope. EBSD orientation imaging maps (OIM) that describe the grain structure in the not-deformed and deformed materials are presented in Figs. 14 – 19. The surface preparation was normal mechanical grinding and polishing with diamond paste followed by OPS polishing as the final step. This preparation showed traces of scratches and it was difficult to prepare the surfaces well for EBSD. Therefore electro-polishing were also carried out and in most maps presented below electro-polishing was used for best results. Electro-polishing was executed in the same way as described earlier; 45 – 60 s in 10 % solution of perchloric acid in methanol at -20°C and 30 V.

Figs. 14 a) and b) describe the not-deformed microstructure in alloy AA6005A. Both figures show OIMs with step length of 10 µm. These OIMs were also used for the texture calculations presented below. Fig. 15 show an OIM of a room temperature deformed specimen (AA6005A). Fig. 16 a) and b) present the microstructure of alloy AA6005A deformed at 500°C. Both images show OIMs with a step length of 1 µm.

Figs. 17 a), and b) describe the not-deformed microstructure in alloy AA6063. In Fig. 17 a) an overview of the microstructure is presented using an OIM with 10 µm step length. In b), a more detailed image of the grain structure is presented. This image was part of a larger OIM. The step length was 2 µm and the information that is included in the image is the colouring according to "Inverse pole figure" (IPF) convention, grain boundaries larger than 15° misorientation (HAGB) (thick black lines) and sub grain boundaries between 2° and 15° misorientation (LAGB) (thin lines. Figs. 18 a) and b) show room temperature deformed material of alloy AA6063. In a) the step length was 1 µm and several grains are included in the figure, the image presents the crystal orientations according to "Inverse pole figure colouring" (IPF), grain boundaries larger than 15° misorientation (HAGB) (thick black lines) and sub grain boundaries between 2° and 15° misorientation (LAGB) (thin lines). In Fig. 18 b) a more detailed OIM is given with 0.25 µm step length; this image is also a part of the larger OIM. LAGB were defined from 1.5° and 15° misorientation in this case. Finally in Fig. 19 a) – c) the microstructure of alloy AA6063 deformed at 500°C is shown. Three OIMs are presented giving examples of differently deformed grains; all three OIMs were scanned using a step length of 0.25 µm. Depending on the crystal orientation the deformation mechanisms and directions have been different, in some cases a clearly seen cell structure has developed, in some cases not.

It is clear that the initial structures are completely equi-axed as is normal in grain refined cast billets. Average grain sizes are about 100µm, slightly larger in AA6005A than in AA6006. A dense internal substructure develops in AA 6005A during straining at room temperature, Fig.15.a), and perhaps less dense in AA6063 although both show evidence of deformation banding in some grains together with general low angle subboundaries. Clearer subgrain formation is evident after the 500°C tests but the tendency varies considerably between different grains, probably depending on their respective orientations in the stress field.

4.1 Textures

Texture calculations were performed for both alloys in the as-received condition using EBSD data for pole figures and ODFs. For both alloys the results showed that the textures were quite isotropic with maximum densities (MUD) of 2.5 (AA6005A) and 2.3 (AA6063). Pole figures for the "overview" OIMs presented in Figs. 14 a) and 17 a) are given in Figs. 20 a) and b). The directions X and Y in the pole figures correspond to the long side and short side of the shear zone geometry (i.e. longitudinal and radial directions in the cast billet). The pole figures do not give reason to believe that there is any strong texture in the materials. If the texture measurement were done over a larger area it is probable that the calculated texture would become even weaker since the number of grains here is probably too few to quantify satisfactorily such a weak texture.

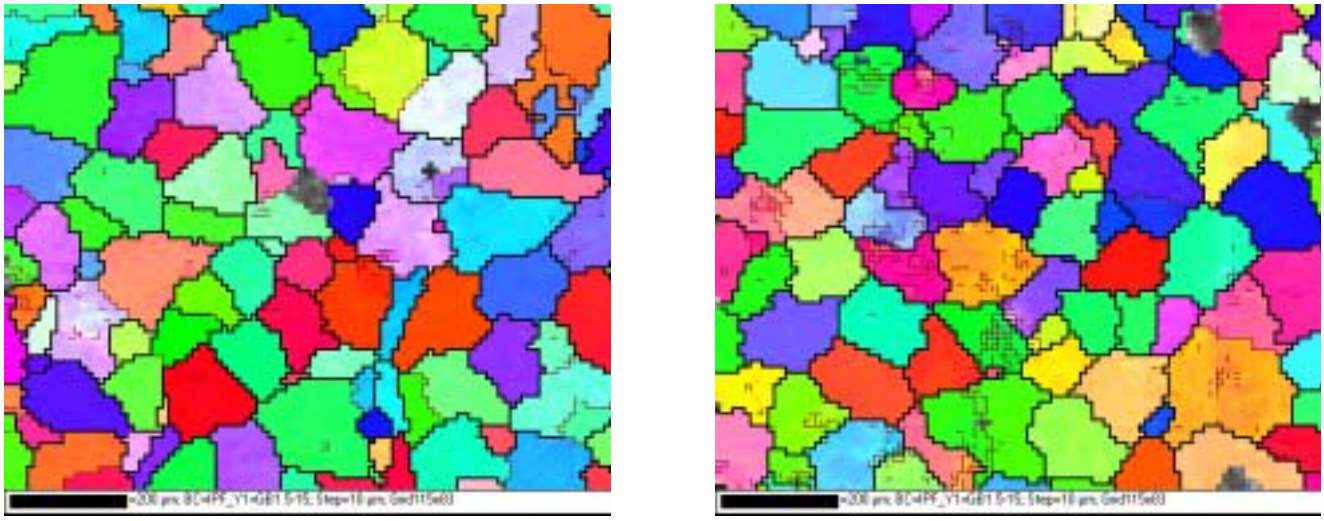

Fig. 14. a), b). Alloy AA6005A not deformed. Both images show an OIM with a step length of 10 µm. The substructure seen in b) is due to effects from surface preparation.

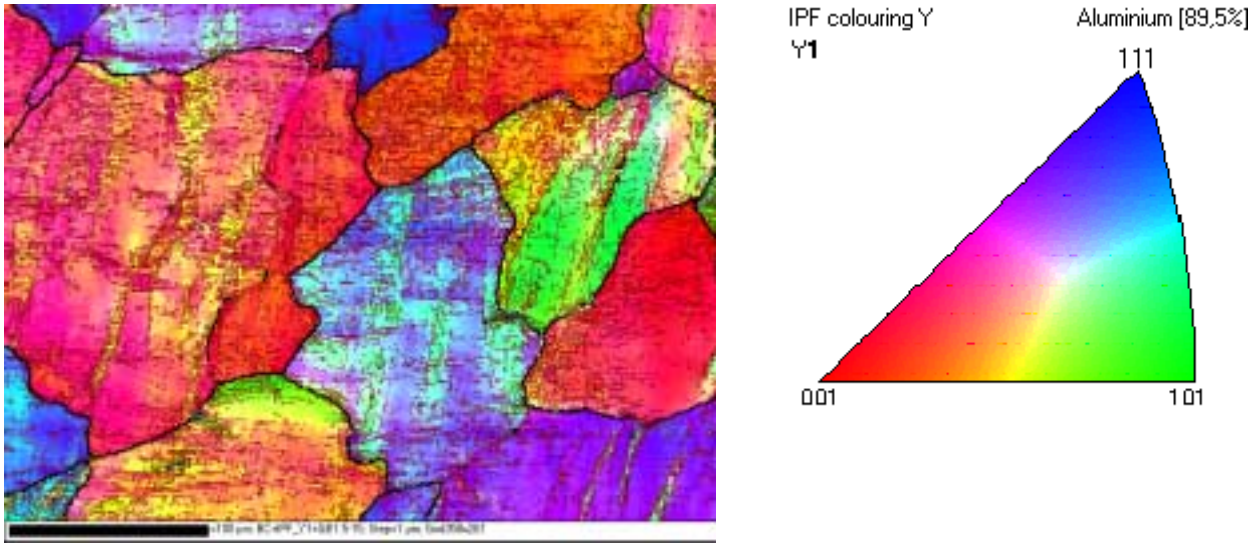

Fig. 15. a), b) Alloy AA6005A deformed at room temperature. OIM with 1 µm step length showing crystallographic direction (colored according to IPF), HAGB (misorientations larger than 15°) and LAGB(misorientations between 2° and 15°). b) key to colouring IPF

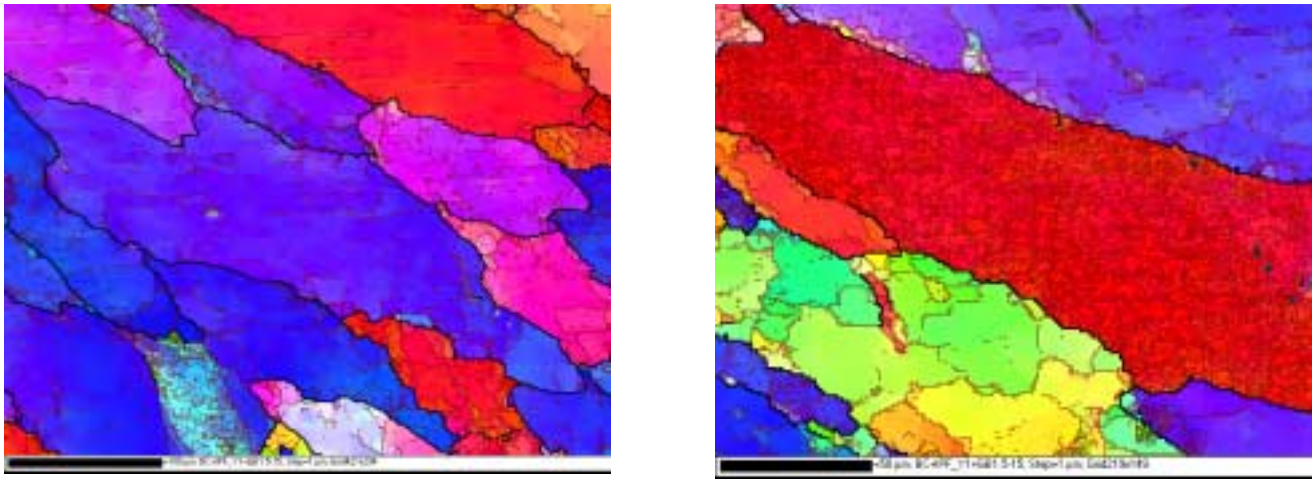

Fig. 16. a), b). Alloy AA6005A deformed at 500°C. Both images show OIMs with a step length of 1 µm is shown.

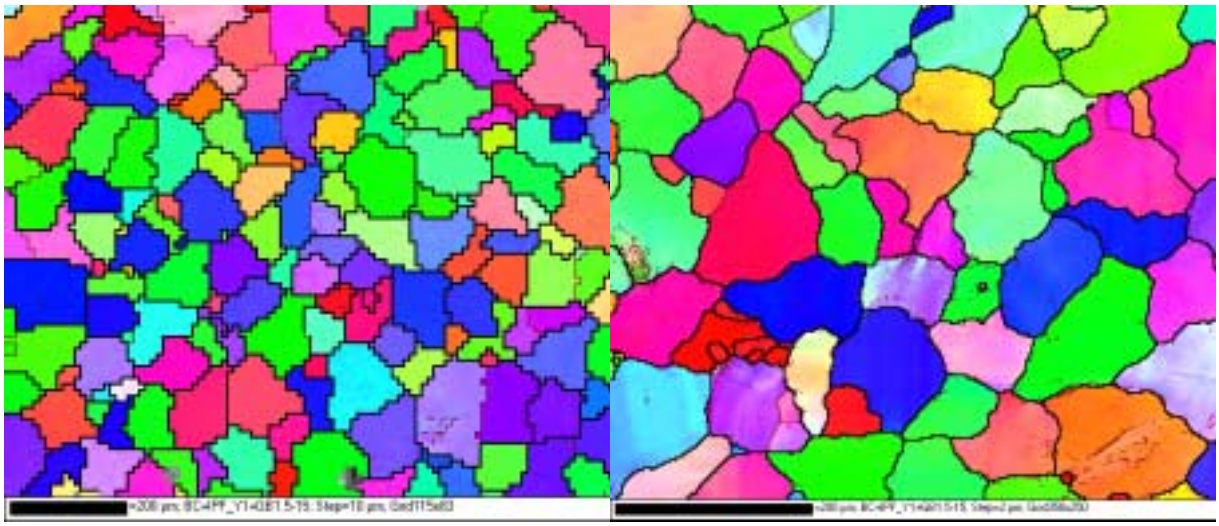

Fig. 17. a), b). Alloy AA6063 not deformed. In a) an overview with a step length of 10 µm is shown, in b) a more detailed OIM with 2 µm step length can be seen.

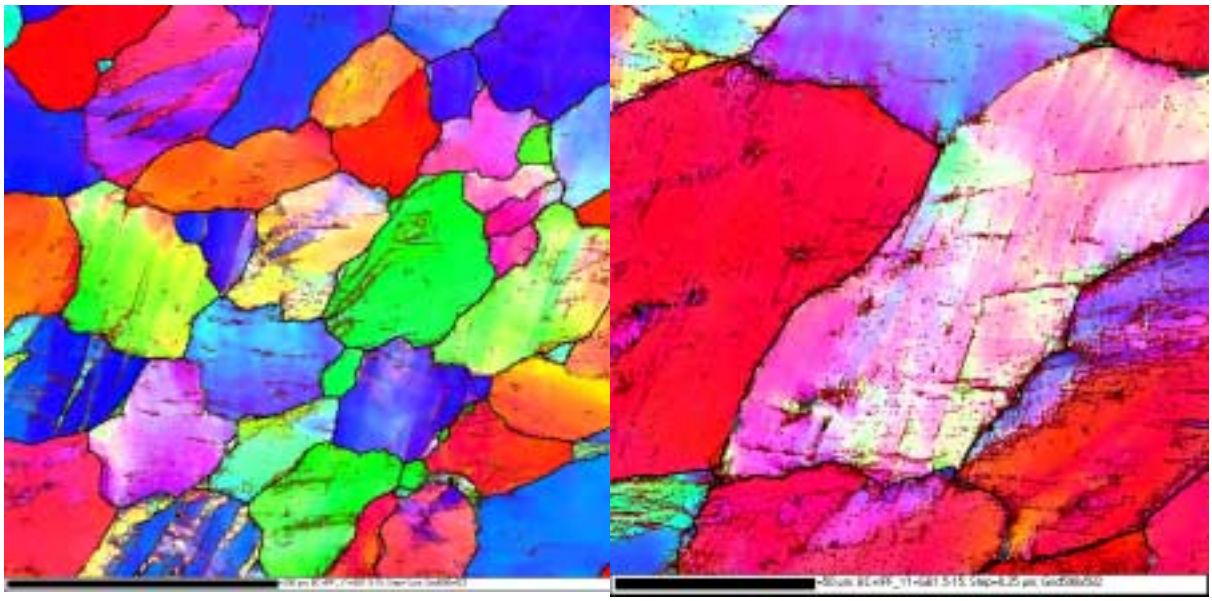

Fig. 18. a), b). Alloy AA6063 deformed at room temperature. In a) an overview with a step length of 2 µm is shown, in b) a more detailed OIM with 0.25 µm step length can be seen.

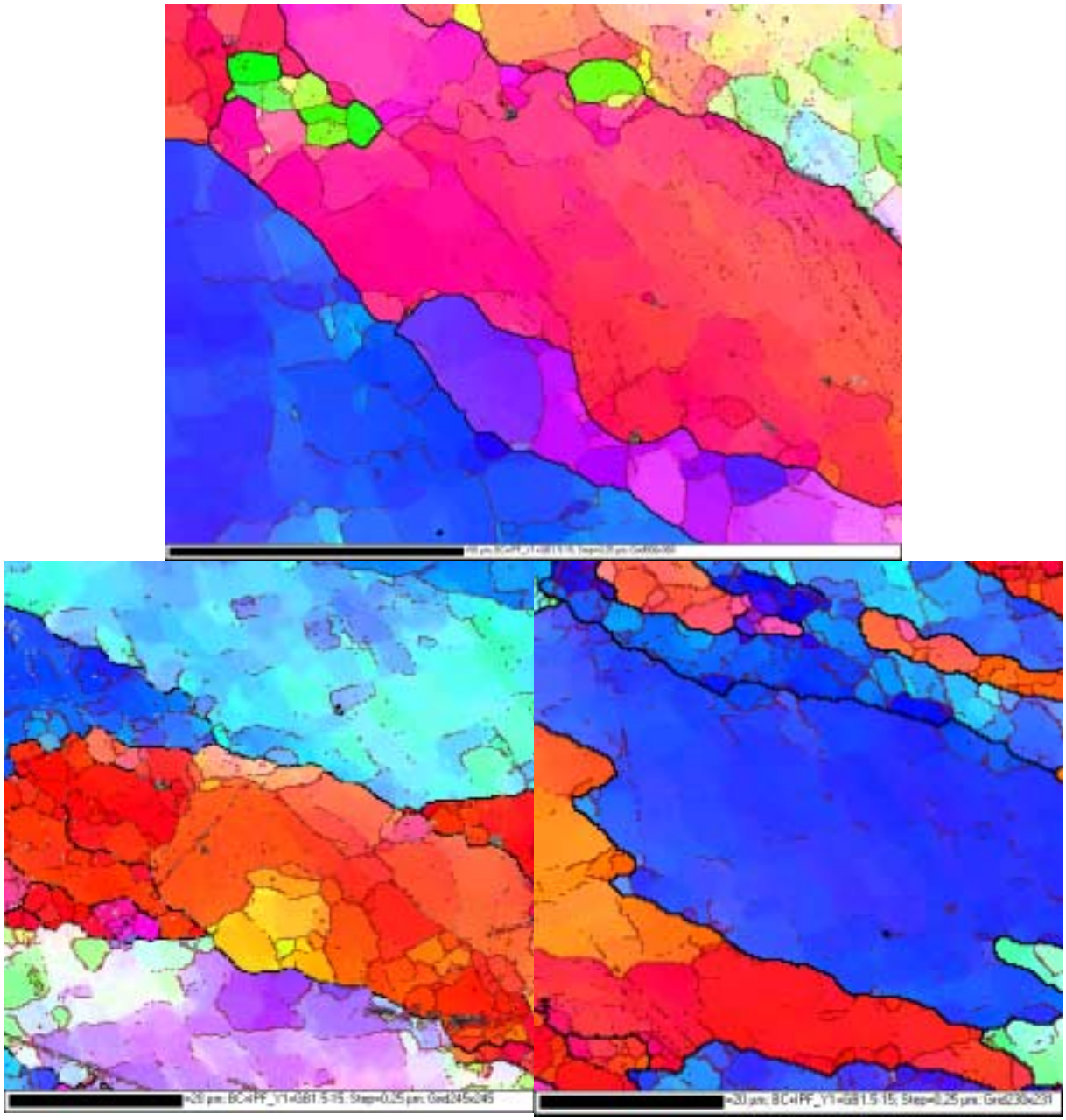

Fig. 19. a) - c). Alloy AA6063 deformed at 500°C. In a) a larger OIM is presented showing a grains that do not contain a lot of substructure. In b) and c) smaller images that were cut from a large OIM that contain several grains with orientations that do develop sub structure and others that do not. 0.25 µm step length in all cases.

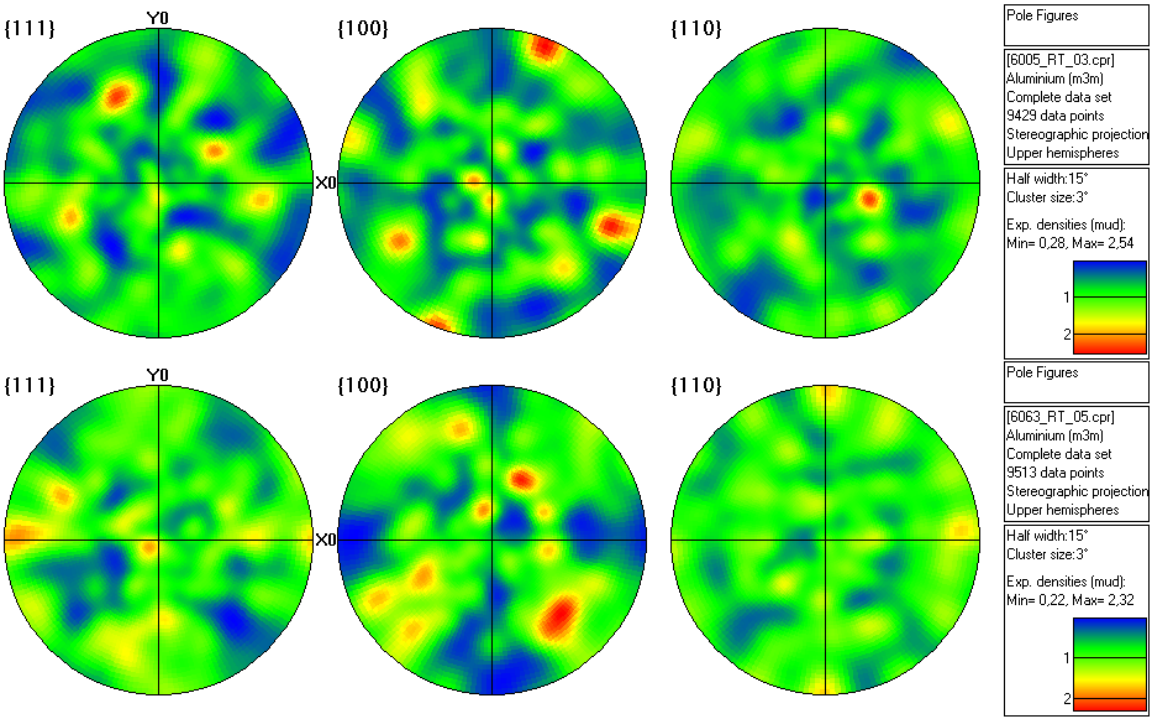

Fig. 20. Pole figures from the OIMs given in Figs. 14 a) and 17 a)

5. Discussion and conclusions

The modifications made to the earlier specimen design have improved the results with respect to localising the measured deformation within the shear zone. Reliable flow stress values can be obtained for shear strains up to 0.5 in room temperature tests and in excess of 0.7 in tests at elevated temperatures relevant to extrusion.

The shear strength of the two alloys was similar at room temperature for small plastic deformations (1 % and 5 %). At higher strains the AA6063 alloy had somewhat higher flow stress which was in agreement with the higher strength in tensile tests measured at Sapa (tensile strengths of 172 MPa and 169 MPa for AA6063 and AA6005A respectively). There was no information on the direction of the tensile tests, so this difference in strength between the alloys could be due to texture differences. In compression tests, the AA6063 material was significantly stronger in the transverse direction (reference to billet length). Alloy AA6005 showed about the same strength in both directions, similar to the strength of alloy AA6063 parallel to the billet length. However, the measured textures of both billet materials were nearly random so the origin of the anisotropy in strength remains something of a mystery

The flow stress decreased with increasing temperature, as expected. At high temperatures, above 400°C, the maximum load decreased with about 0.1 MPa/°C. The temperature dependence at room temperature was higher, since the flow stress drop between room temperature and 400°C was about 80 to 85 MPa, corresponding to more than 0.2 MPa/°C. The preceding project found that the flow stress decreased steadily from room temperature to 550°C, but then increased slightly from 550°C to 600°C. This behaviour was not seen in the results obtained here. At 600°C both alloys showed normal stress-strain curves, although at very low stress levels. The maximum shear stresses at 600°C were 15 MPa and 13.5 MPa respectively for alloy AA6005A and AA6063.

The flow stress increased with increasing strain rate, as expected. At room temperature the increase was moderate ($d\sigma / d\log(\dot{\varepsilon}) \approx 1$) but at high temperatures the increase was much larger ($d\sigma / d\log(\dot{\varepsilon}) \approx 7$). Compared to the initial strength this increase at high temperatures was very large. For example, the yield stress (at 5 % elongation) was 7,75 MPa for alloy AA6063 at 600°C and 1/s strain rate and increased by 6,75 MPa when the strain rate was 100/s. The flow stress thus increased 90 % to 14,5 MPa when the strain rate increased from 1/s to 100/s. The flow stress increase at room temperature was only 1 % for a similar change in strain rate.

In the high temperature regime the flow stresses can be described by the following expressions (von Mises effective strain):

$$\sigma_{pl} = \sigma_0 + k\varepsilon_{pl}^n \qquad \text{Eq. 2}$$

$$\sigma_2 = \sigma_1 + k\log\left(\dot{\varepsilon}_2 / \dot{\varepsilon}_1\right) \qquad \text{Eq. 3}$$

$$T^* = \frac{T - T_{ref}}{T_{melt} - T_{ref}} \qquad \text{Eq. 4}$$

$$\sigma = \sigma_{ref}\left(1 - \left(\frac{T - T_{ref}}{T_{melt} - T_{ref}}\right)^m\right) \qquad \text{Eq. 5}$$

Ductility increased moderately with temperature, measured as the strain at which cracks started to develop. The shear strain increased from 0.5 mm/mm at room temperature to 0.9 mm/mm at 600°C.

Alloy AA6063 was ductile up to the highest measured temperature of 625°C, but alloy AA6005A failed at the highest temperature where the specimen collapsed at very low load and displacement as the material had begun to melt at that temperature. This demonstrates the possibility of using the present test procedure as a critical measure of hot workability since the temperature is known quite accurately and so combinations of temperature and strain/strain rate where collapse occurs can be detected. This would be an interesting aspect to take up in future work.

Comparison of the shear tests with compression tests on the same materials at room temperature reveals some quite large differences after converting the measured values to von Mises effective stresses and strains (we ignore here any behaviour at deformations after the on-set of crack formation in shear as these values are clearly not trustworthy). At small strain levels the agreement is close but the curves diverge subsequently and the flow stress in compression is some 20% higher than for shear at a strain of 0.3. There may be several sources for this deviation. Firstly, the von Mises expression has no physical basis and does not conform exactly to crystal plasticity models such as that of Taylor even in the absence of texture. During deformation there is a progressive development of texture which leads to geometrical hardening in compression and to geometrical softening in shear. This is probably an important contribution to the observed behaviour. Thirdly, tensile tests demonstrated differences in stress level for different test directions in the billets, especially for AA6063. Although the origin of this anisotropy has not been established, it could have contributed to the difference found between compression and shear. Finally, there were indications on some of the compression test curves that the effect of end friction may not be completely compensated. Since the deformation in extrusion constitutes strain states that resemble much more closely shear than compression, there is good reason to believe that the flow behaviour evaluated from shear tests will be more relevant and, therefore, more appropriate for use in finite element modelling of industrial processes.

6. References

[1] Hagström, J., ”*Skjuvprovning av aluminiumlegeringar vid olika temperaturer och töjningshastigheter”,* KIMAB-2006-105
[2] Metals Handbook, ASM international
[3] Properties and Physical Metallurgy, J. E. Hatch, 1984
[4] Handbok för konstruktörer, SAPA, 1995
[5] Hagström J and Lindh-Ulmgren E., ”*Materialegenskaper vid höga töjningshastigheter”,* IM-2000-006, 2000
[6] Hatherley, M. and Hutchinson B., An introduction to Textures in Metals, Monograpg no 5, The institution of Metallurgists